Wireless Power Transfer

ARTICLE

Open Access

https://doi.org/10.48130/wpt-0024-0019

Wireless Power Transfer **2025**, 12: e006

Efficiency control for multi-receiver inductive power transfer systems without knowing realtime coupling

Xinlin Wang, Rong He, Ziyuan Lin and Minfan Fu*

School of Information and Technology, ShanghaiTech University, Shanghai 201100, China

* Corresponding author, E-mail: fumf@shanghaitech.edu.cn

Abstract

This study is centered on maintaining high efficiency within a multi-receiver system in the absence of real coupling information. It explores the derivation of an optimal driving current crucial for efficiency maximization, revealing its reliance on both loading and coupling conditions. Furthermore, an average current is defined based on known coupling ranges, typically accessible during the system's design phase. Employing this derived driving current significantly enhances system scalability with minimal additional requirements in communication, state estimation, and activating circuits. In an experimental setup, a two-receiver system is constructed to contrast the efficiency achieved when possessing real-time coupling knowledge vs solely knowing the coupling range. The observed maximum efficiency difference between these scenarios amounts to 1.7%.

Citation: Wang X, He R, Lin Z, Fu M. 2025. Efficiency control for multi-receiver inductive power transfer systems without knowing realtime coupling. *Wireless Power Transfer* 12: e006 https://doi.org/10.48130/wpt-0024-0019

Introduction

In recent years, the widespread use of intelligent mobile terminals has been driving the process of societal intelligence. However, wired charging based on manual connections will severely limit this development[1]. Inductive power transfer (IPT) has emerged as a promising remedy for charging these intelligent terminals, enabling efficient power transmission from a transmitter (TX) to a receiver (RX). Presently, research focusing on single-TX single-RX IPT systems has achieved considerable maturity. Substantial advancements have been accomplished in coil design, compensation network configuration, output control, efficiency enhancement, and the detection of foreign objects[2–4]. These developments greatly support the expansion and application of this technology.

Multi-RX charging has emerged as an attractive and challenging area of research. Varied application scenarios present distinct system characteristics, necessitating a focused approach towards system-level design adaptable to diverse power requirements and coupling conditions. In addressing these challenges, extensive discussions have centered around coupler designs, leading to the development of various structures aimed at enhancing and stabilizing the coupling amidst diverse misalignment scenarios[5,6]. Furthermore, the compensation networks have been recognized as crucial for attaining multiple objectives, including minimizing circulating energy, facilitating soft switching in active circuits, and ensuring output stability amidst load variations[7]. Notably, beyond passive circuitry, significant progress has been achieved in active circuit designs tailored for multi-RX scenarios[8,9]. These advancements in coupler and activating circuit designs serve as foundational requisites ensuring the steady-state performance of the system.

A well-performed multi-RX system necessitates an intelligent control methodology to fully exploit its potential benefits. The key control objectives primarily encompass output regulation, power distribution among RXs, and efficiency optimization. For instance, in cases where each RX possesses a specific resonance frequency, employing multiple-frequency excitation allows for independent power control across multiple RXs[10–12]. The overall efficiency is enhanced in the study by Kim et al.[13] through the computation of the optimal TX driving current, which heavily relies on the RX-side circuitry and real-time communication. Similarly, a communication-based control strategy has been devised for a system driven by a single Class E inverter, aiding in achieving simultaneous power and efficiency modulation[14]. Various input modes are formulated in the study of Zhao et al.[15] to optimize efficiency and cater to diverse power demands. However, these systems predominantly address specific scenarios, failing to comprehensively portray the inherent trade-offs and natural dependencies between achieved performance metrics (such as efficiency and power) and the requisite system complexity (e.g., real-time communication, information sensing, computational burden, and activation of circuits).

This manuscript centers on upholding high efficiency within a single-TX multi-RX system, without knowing real coupling. Employing the single-TX scenario as a case study, the examination delves into the impact of terminal conditions—specifically, the driving current and load—on the resonant tank. This investigation then steers the discourse towards an in-depth analysis of existing approaches aimed at maximizing efficiency at different power. In the absence of real-time coupling knowledge, an optimal current is deduced based on pre-established coupling ranges. As the number of RX grows, the suggested driving logic exhibits considerable scalability and an elevation in system intricacy. The attained efficiency under complete knowledge of all couplings stands as the reference point, only marginally surpassing the efficiency attained through the proposed control strategy.

Single receiver system

System characteristics

The depicted single-TX single-RX IPT system, shown in Fig. 1, encompasses essential components such as the inverter, coupler, compensation unit, rectifier, and load, which collectively elucidate the fundamental control logic. The active circuits, including the inverter, rectifier, and DC/DC converters in both the front-end and post stages, enable input and output modulation for diverse control objectives. Within this system, L_{tx} and r_{tx} denote the self-inductance

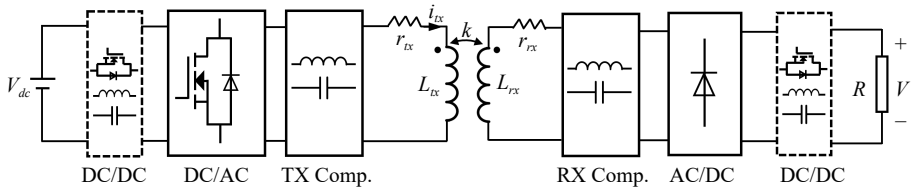

Fig. 1 Configuration of 1TX-1RX system.

and equivalent series resistance (ESR) of the TX coil, respectively, while L_{rx} and r_{rx} represent the self-inductance and ESR of the RX coil. The symbol M signifies the mutual inductance between the coils, while the coefficient k is defined as the coil coupling coefficient: $k = \frac{M}{\sqrt{L_{tx}L_{rx}}}$.

In Fig. 1, both the TX and RX sides should offer at least two control variables to adjust the output and optimize efficiency indirectly. Typically, these control variables encompass the duty cycle of the DC/DC converter, and the phase shift angle of the inverter, or rectifier. Different combinations of these variables yield various control configurations, as documented in prior studies[16–18]. Under specific output conditions, such as maintaining a constant voltage (CV), the controllable circuits must satisfy the load's power requirements while ensuring high efficiency throughout the entire system. When dealing with a system incorporating an uncontrollable resonant tank, the diverse configurations and control strategies mentioned earlier can be simplified and clarified through a steady-state analysis of the central resonant tank. This analysis focuses specifically on the integration of compensation and coupler elements and hinges upon terminal conditions—specifically, the input from the TX side and the load output on the RX side.

Despite the existence of various compensations, if assume that losses within the coupler exert a dominant influence on the overall losses, then the efficiency wouldn't be significantly impacted by compensation on the TX side. Consequently, this study is aimed at investigating the passive network depicted in Fig. 2, where TX compensation is disregarded, and a straightforward series compensation is implemented on the RX side. In this setup, C_{rx} denotes the series compensating capacitor, fulfilling the condition $1/(\omega C_{rx}) = \omega L_{rx}$, while i_{tx} represents the input current to the TX coil.

In terms of the load viewpoint, controllable systems can be classified into two distinct types. The first type involves manipulating the RX-side circuitry to attain the optimal load while simultaneously adjusting the TX-side excitation to fulfill the output power requirements, as illustrated in Fig. 2a. In this arrangement, the rectifier and its subsequent circuit components are treated as a load resistance $R_{rx,opt}$ when aiming for maximum coupler efficiency. The RX's output power during resonance is expressed as:

$$P_o = \left(\frac{\omega M I_{tx}}{R_{rx,opt} + r_{rx}}\right)^2 R_{rx,opt} \tag{1}$$

The optimal load resistance $R_{rx,opt}$ for efficiency maximization has been well studied and derived as:

$$R_{rx,opt} = r_{rx}\sqrt{1 + \frac{\omega^2 M^2}{r_{tx} r_{rx}}} \tag{2}$$

By solving Eqns (1) and (2) concurrently, it gives the root mean square (RMS) value of the necessary input current under the optimal condition, expressed as follows:

$$I_{tx,ropt} = \frac{\sqrt{P_o}}{\omega M}\sqrt{2r_{rx} + \frac{2r_{tx}r_{rx} + \omega^2 M^2}{\sqrt{r_{tx}r_{rx} + \omega^2 M^2}}\sqrt{\frac{r_{rx}}{r_{tx}}}} \tag{3}$$

The efficiency of the coupler is:

$$\eta_{c,ropt} = 1 - \frac{2}{\sqrt{1 + \frac{\omega^2 M^2}{r_{tx} r_{rx}}} + 1} \tag{4}$$

which is loading and coupling dependent.

The second type of system aims to provide optimal driving current to maximize efficiency, and its load model is illustrated in Fig. 2b. In this setup, the RX-side circuit maintains the desired output characteristics, such as a constant voltage (CV), while satisfying specific power requirements P_o through RX-side control. Simultaneously, the TX-side circuit adjusts the input excitation to enhance efficiency. Despite the differing control methodologies between these two types, the eventual steady-state effects remain consistent. The primary difference lies in the approaches used to achieve this optimal state, involving distinctions in the activation of circuits, communication protocols, and the requisite information, particularly the coupling.

In Fig. 2b, maximizing efficiency is equivalent to minimizing losses for a target power. The power loss is expressed as:

$$P_{\text{loss}} = P_{\text{loss,tx}} + P_{\text{loss,rx}} = I_{\text{tx}}^2 r_{\text{tx}} + I_{\text{rx}}^2 r_{\text{rx}} \tag{5}$$

The optimal excitation at this point can be determined by solving the equation $\frac{dP_{\text{loss}}}{dI_{\text{tx}}} = 0$, yielding the coil's input current excitation $I_{\text{tx,iopt}}$, which would further determine the corresponding optimum efficiency $\eta_{c,iopt}$. Based on derivation, it would find $I_{\text{tx,iopt}} = I_{\text{tx,ropt}}$ and $\eta_{c,iopt} = \eta_{c,ropt}$. The fact that both types of systems share the same excitation in the steady state indicates that, despite different control methods and transient processes, the systems reach identical stable states, i.e., there exists only one global maximum efficiency point. If $R_{rx,opt} \gg r_{rx}$, the losses on the TX and RX coils are equal and can be expressed as:

$$P_{\text{loss,tx}} \approx P_{\text{loss,rx}} = \frac{P_o}{\sqrt{1 + \frac{\omega^2 M^2}{r_{\text{tx}} r_{\text{rx}}}}} \tag{6}$$

It physically means the optimal efficiency indicates a loss balance condition.

By employing optimal load control as illustrated in Fig. 2a, achieving $R_{rx,opt}$ demands coupling information for the RX, while the TX relies on receiving feedback (usually via wireless communication) from the RX to regulate power[19]. Conversely, using the second approach depicted in Fig. 2b allows independent regulation of the RX through a linear controller. In the absence of communication, the TX must resort to either a non-linear tracking algorithm or a sensing-based coupling estimation approach to provide the necessary

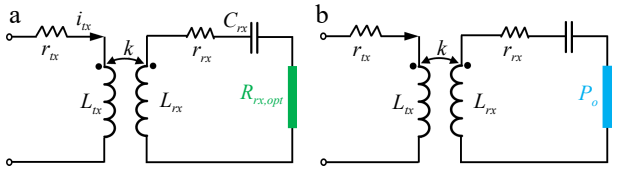

Fig. 2 Equivalent circuit under different control strategies. (a) Optimal load. (b) Optimal excitation.

optimal driving current[20]. Consequently, a noticeable trade-off emerges involving the communication requirement, controller type, and sensing necessity.

Excitation current based on coupling range

This paper presents a simplified excitation control approach based on the coupling range. The proposed method simplifies the control process by requiring determination of the coupling coefficient range during the coupler design phase. Following implementation, the system operates autonomously, obviating the necessity for real-time coupling estimation or nonlinear tracking algorithms. The core operational principle is demonstrated initially in a straightforward single-RX scenario, subsequently extending its applicability to a more intricate multi-RX scenarios.

In a single-RX system, ensuring sufficient coupling generally requires the RX to be charged within a specified charging area. In such instances, the range of coupling coefficient variations is limited and becomes known upon the fabrication of the coupler. The controllable circuit on the RX side can uphold a constant voltage output (fulfilling the load power requirements), while the TX side employs a real-coupling-independent control. The excitation current is determined by the range of coupling variations.

Figure 3 illustrates the efficiency curve of the coupler, demonstrating variations in input currents while regulating the RX side to achieve the target power. Within the graph, $M_{\min}$ signifies the minimum mutual inductance, $M_{\max}$ signifies the maximum mutual inductance, P_o represents the output power, and the upper and lower boundaries are established by the coupling range. The solid black line represents the system response at maximum coupling, while the solid red line represents the system response at minimum coupling. Within the determined coupling range, the actual response curve of the system is denoted by the dashed blue line. Given offset conditions, the blue line remains constrained within the upper and lower boundaries.

In Fig. 3, L denotes the optimal efficiency point when the coupling is at its minimum. According to Eqn (3), this point is associated with an optimal input excitation, $I_{tx,L}$, given by:

$$I_{tx,L} = \frac{\sqrt{P_o}}{\omega M_{\min}} \sqrt{2r_{rx} + \frac{2r_{tx}r_{rx} + \omega^2 M_{\min}^2}{\sqrt{r_{tx}r_{rx} + \omega^2 M_{\min}^2}} \sqrt{\frac{r_{rx}}{r_{tx}}}} \tag{7}$$

Here, H corresponds to the optimal point when the coupling is at its maximum, associated with an optimal excitation, $I_{tx,H}$, given by:

$$I_{tx,H} = \frac{\sqrt{P_o}}{\omega M_{\max}} \sqrt{2r_{rx} + \frac{2r_{tx}r_{rx} + \omega^2 M_{\max}^2}{\sqrt{r_{tx}r_{rx} + \omega^2 M_{\max}^2}} \sqrt{\frac{r_{rx}}{r_{tx}}}} \tag{8}$$

If employing the non-linear perturbation observation method, the system requires continuous tracking of the optimal excitation between $I_{tx,L}$ and $I_{tx,H}$[21]. Despite the absence of direct communication between the TX and RX sides, disturbances on the TX side can affect the stability of the RX side output. In scenarios without nonlinear tracking, estimating the coupling based on TX side information becomes necessary to maintain the coupling-dependent optimal current[20].

Within the specified coupling range, this paper proposes a strategy that utilizes the average of $I_{tx,L}$ and $I_{tx,H}$ as the driving current, denoted as:

$$I_{tx,M} = \frac{I_{tx,L} + I_{tx,H}}{2} \tag{9}$$

The median current value, $I_{tx,M}$, is influenced by coil parameters, load power, and the coupling range. When the real coupling is $M_{\min}$, the operating point becomes L' using $I_{tx,M}$ as the driving current. The efficiency difference between L' and L is $\Delta\eta_{C,L}$. Conversely, at maximum coupling, the operating point is H', and the efficiency difference between H' and H is $\Delta\eta_{C,H}$. $\Delta\eta_{C,L}$ and $\Delta\eta_{C,H}$ depict the trade-off incurred by using the real-coupling-independent $I_{tx,M}$.

The proposed excitation control strategy eliminates the necessity for real-time tracking of the highest efficiency point and instead maintains operation at a compromise point. At this juncture, the TX side losses stabilize at $I_{tx,M}^2 \cdot r_{tx}$, and different couplings determine varying currents on the RX-side coil. When the current on the RX-side coil reaches a certain value such that the losses at both ends of the coil become equal, i.e., $I_{tx,M}^2 \cdot r_{tx} = I_{rx}^2 \cdot r_{rx}$, the system attains its actual maximum efficiency point.

Influence of coupling range

To provide a quantitative verification and study the impact of the coupling range, a simulation is employed for further elucidation of the qualitative analysis. The simulation utilizes the following parameters: f = 100 kHz, L_{tx} = 90 μH, L_{rx} = 75 μH, r_{tx} = 0.192 Ω (Q_{tx} = 250), r_{rx} = 0.174 Ω (Q_{rx} = 230), and P_o = 20 W. As the coupling varies, the coupler efficiency changes with the input excitation, as depicted in Fig. 4. Region A delineates the operational area when k ranges within [0.1,0.2]. The simulation results indicate that with an increase in k, the corresponding optimal excitation current decreases.

If the driving current is controlled to be the optimal value, i.e., $I_{tx} = I_{tx,opt}$, the efficiency is depicted by the black dashed line in Fig. 5, which connects all peak points of Fig. 4. This reference curve serves as the basis for analyzing the influence when I_{tx} changes to $I_{tx,M}$. For instance, considering $k \in [0.1, 0.2]$, the efficiency achieved by $I_{tx,M}$—calculated using Eqns (7), (8), and (9)—is represented as case A (yellow solid line) in Fig. 5. It marginally falls below the reference curve, with a maximum drop of 0.5%. Expanding the coupling range to $k \in [0.08, 0.2]$, corresponding to the region between the green and blue solid lines of Fig. 4, yields the efficiency achieved by $I_{tx,M}$ represented as case B in Fig. 5, exhibiting a maximum drop of 1%. When $k \in [0.06, 0.2]$, as demonstrated in case C, it results in a maximum 2% efficiency drop. These simulation outcomes indicate that adopting $I_{tx,M}$ based on the coupling range demonstrates efficiency

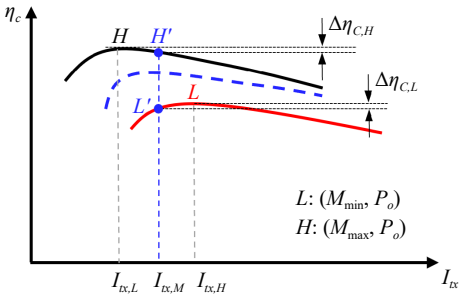

Fig. 3 Coupler efficiency at different k and I_{tx}.

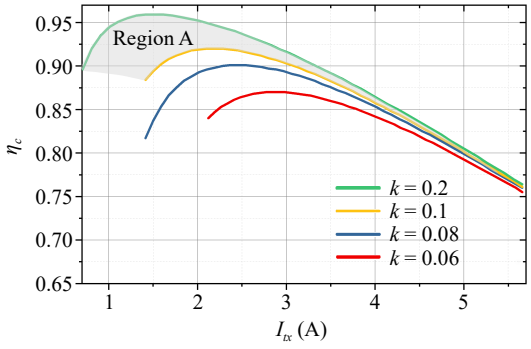

Fig. 4 Efficiency of the 1-RX system under different coupling conditions.

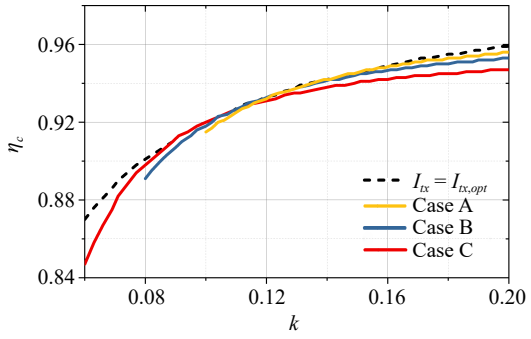

Fig. 5 Efficiency when the coupling range changes.

performance close to real-time tracking of the optimal excitation, showcasing favorable system characteristics.

Multi-RX system

System characteristic and optimal driving current

Figure 6 illustrates a single-TX n-RX system. $L_{rx,j}$ and $r_{rx,j}$ denote the self-inductance and ESR of the j-th RX coil. k_j is the coupling coefficient between the TX and the j-th RX, satisfying: $k_j = M_j/\sqrt{L_{tx}L_{rx,j}}$. $C_{rx,j}$ is the series compensation capacitor, and $R_{rx,j}$ is the equivalent AC load resistance. The resonance on the RX side satisfies the condition: $\omega L_{rx,j} - 1/(\omega C_{rx,j}) = 0$. In scenarios where charging occurs in a flat plane, having multiple RXs positioned over the TX charging area can induce cross-coupling between the RXs. Since the RX coil is enclosed within the device, the minimum coil clearance between adjacent devices becomes a variable during the design phase. Adequate clearance between coils is essential to minimize cross-coupling effects. Consequently, the analysis conducted above assumes a model where the RX cross-coupling is not considered.

Similar to the single RX scenario depicted in Fig. 2, when employing different control logics in RXs, it becomes essential to individually examine the optimal conditions achieved. In scenarios where the system offers multiple control options, adjusting the load resistance at each RX becomes crucial to maximize coupler efficiency. As outlined in the study by Fu et al.[22] , the necessary load resistance values and their respective efficiencies are:

$$R_{rx,j,opt} = r_{rx,j}\sqrt{1+\sum_{j=1}^{n}\frac{\omega^2 M_j^2}{r_{tx}r_{rx,j}}} \tag{10}$$

$$\eta_{c,ropt} = 1 - \frac{2}{\sqrt{1+\sum_{j=1}^{n}\frac{\omega^2 M_j^2}{r_{tx}r_{rx,j}}}+1} \tag{11}$$

In contrast to the single-RX system, the aforementioned multi-RX system possesses n power outputs and n optimal load resistance values. It offers n + 1 degrees of freedom for control, provided by

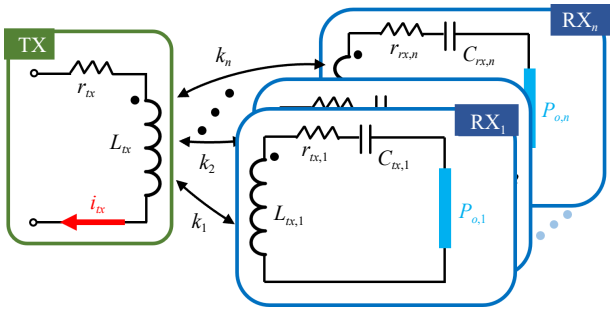

Fig. 6 Simplified circuit model of one-TX n-RX system.

the TX and RX sides (n on the RX side, 1 on the TX side). To achieve global optimal efficiency, i.e., satisfy Eqn (11), each load should adhere to the optimal load condition, i.e., Eqn (10), through its respective control circuit. In this scenario, the power distribution among the loads is constrained to follow the following proportions:

$$P_1 : P_2 : \cdots : P_n = \frac{M_1^2}{r_{rx,1}} : \frac{M_2^2}{r_{rx,2}} : \cdots : \frac{M_n^2}{r_{rx,n}} \tag{12}$$

There are no degrees of freedom available for power regulation. Therefore, the control logic of Fig. 2a cannot be extended to a multi-RX scenario.

When the RX-side circuit is dedicated to maintaining a constant voltage, the excitation current on the TX side becomes pivotal in enhancing the system's efficiency. This reflects the optimal excitation control employed in a scenario featuring a single TX and a single RX. In this context, maximizing the system's efficiency can be reformulated as a problem centered on minimizing losses while adhering to equality constraints, as articulated below:

$$\begin{aligned} &\text{Minimize}: \quad I_{tx}^2 r_{tx} + \sum_{j=1}^{n}\left(\frac{\omega M_j I_{tx}}{R_{rx,j}+r_{rx,j}}\right)^2 r_{rx,j} \\ &\text{Subject to}: \quad \left(\frac{\omega M_j I_{tx}}{R_{rx,j}+r_{rx,j}}\right)^2 R_{rx,j} = P_j, \quad j = 1,2,...,n \end{aligned} \tag{13}$$

The method for solving such an optimization problem involves the Lagrange multiplier method. Equation (14) represents the Lagrangian, where L is the Lagrange function, and λ_j is the Lagrange multiplier.

$$L = I_{tx}^2 r_{tx} + \sum_{j=1}^{n}\left(\frac{\omega M_j I_{tx}}{R_{rx,j}+r_{rx,j}}\right)^2 r_{rx,j} + \sum_{j=1}^{n}\lambda_j\left(\left(\frac{\omega M_j I_{tx}}{R_{rx,j}+r_{rx,j}}\right)^2 R_{rx,j} - P_j\right) \tag{14}$$

If $R_{rx,opt} \gg r_{rx}$, by solving $\frac{\partial L}{\partial I_{tx}} = 0$ and $\frac{\partial L}{\partial \lambda_j} = 0$, the optimal input excitation current I_{tx}, of the system under known coupling coefficients, which maximizes system efficiency, can be obtained as follows:

$$I_{tx,opt} = \left(\frac{1}{r_{tx}}\sum_{j=1}^{n}\frac{P_j^2 r_{rx,j}}{\omega^2 M_j^2}\right)^{\frac{1}{4}} \tag{15}$$

Substituting Eqn (15) into the efficiency expression yields:

$$\eta_{c,iopt} = \frac{\sum_{j=1}^{n} P_j}{\sum_{j=1}^{n} P_j + 2\left(\sum_{j=1}^{n}\frac{P_j^2 r_{rx,j}}{\omega^2 M_j^2}\right)^{\frac{1}{2}}} \tag{16}$$

At this point, the coupler achieves an efficiency $\eta_{c,iopt}$ while facing power constraints on the RX side, rather than the globally optimal efficiency $\eta_{c,ropt}$ obtained without power constraints, expresses the system efficiency when operating at the global optimum, representing the theoretical efficiency limit of the system. Therefore, $\eta_{c,iopt} \leq \eta_{c,ropt}$, signifying that under the control strategy of optimal excitation, the efficiency is always lower than the efficiency under optimal load conditions. The losses on the TX and RX sides at this point are given by:

$$P_{loss,tx} = P_{loss,rx} = \left(\sum_{j=1}^{n}\frac{P_j^2 r_{rx,j}}{\omega^2 M_j^2}\right)^{\frac{1}{2}} \tag{17}$$

This conclusion indicates that under optimal excitation, the coil conduction losses on the TX side and RX side are equal, consistent with the characteristics of a single-RX system [refer to Eqn (5)].

From the above analysis, it can be concluded that for a general multi-RX system with different RX coils, various couplings, and distinct power requirements, when the coil parameters and output power are determined, the coupler efficiency depends solely on the

coupling and the input excitation I_{tx}. This characteristic is akin to the single-RX case. Despite the increase in the number of outputs, the control freedom of TX remains unchanged. The upper and lower boundaries of the efficiency curve are still determined by the coupling variation range. Therefore, the efficiency curve shown in Fig. 4 is still applicable to a multi-RX system. The red solid line represents the efficiency curve when the coupling between the TX and all RXs is minimized (i.e., $M_j = M_{min}$). At this point, the current at the efficiency peak L is given by:

$$I_{tx,L} = \left(\frac{1}{r_{tx}} \sum_{j=1}^{n} \frac{P_j^2 r_{rx,j}}{\omega^2 M_{\min}^2} \right)^{\frac{1}{4}} \tag{18}$$

The black solid line represents the efficiency curve when the coupling between the TX and all RXs is maximized (i.e., $M_j = M_{max}$). The current at the corresponding efficiency peak is given by the following:

$$I_{tx,H} = \left(\frac{1}{r_{tx}} \sum_{j=1}^{n} \frac{P_j^2 r_{rx,j}}{\omega^2 M_{\max}^2} \right)^{\frac{1}{4}} \tag{19}$$

It is possible to adopt the average current, which mirrors the approach used in the single-RX system, i.e.,

$$I_{tx,M} = \frac{I_{tx,L} + I_{tx,H}}{2} \tag{20}$$

which is also influenced by coil parameters, load power, and the coupling range. Given the known coupling range, the input excitation is determined without the need for real-time coupling information. When using the proposed excitation, the TX coil loss is $P_{loss,tx} = I_{tx,M}^2 R_{tx}$, while the RX-side losses vary with the coupling. When the coupling changes to the condition given by Eqn (17), where the sum of RX-side losses equals the TX side losses, the system reaches its optimal efficiency state, calculated as Eqn (16).

In a single-RX system, the TX side must obtain specific coupling and load information through communication or detection means and then calculate the optimal excitation. Similarly, in a multi-RXs system, if coupling estimation or similar methods are employed, the difficulty of estimating information and the circuit cost will increase dramatically due to the addition of RX devices. Therefore, the proposed driving strategy would show great scalability and is particularly advantageous in multi-RX systems.

Influence of coupling range

Taking the example of a dual-RX system to study the influence of coupling, Table 1 shows the simulation parameters. The coupling range is $k_1 \in [0.1, 0.34]$ for RX1, and $k_2 \in [0.15, 0.45]$ for RX2. In Fig. 7, when meeting the power demand, the coupler efficiency changes with input excitation, and different colors represent different coupling conditions. The blue line represents the coil efficiency change curve when the coupling is strongest ($k_1 = 0.2$, $k_2 = 0.25$), the orange curve represents an intermediate state ($k_1 = 0.34$, $k_2 = 0.45$), and the black solid line is used to represent the weakest coupling ($k_1 = 0.1$, $k_2 = 0.15$). Similar to Fig. 4, stronger coupling leads to a smaller optimal excitation current and higher efficiency. Additionally, the power level and coil parameters also influence the shape and position of the efficiency curve.

Table 1. Parameters of 1TX-2RX IPT system.

Symbol	Value	Symbol	Value	Symbol	Value
f	100 kHz	L_{tx}	91.3 μH	r_{tx} & r_{rx}	0.195 Ω
$L_{rx,1}$	22.3 μH	$r_{rx,1}$	0.059 Ω	k_1	[0.1, 0.34]
$L_{rx,2}$	26.4 μH	$r_{rx,2}$	0.074 Ω	k_2	[0.15, 0.45]
P_1	15 W	P_2	10 W		

Analogous to the single-RX system, for certain spatial offsets in practical applications, real-coupling-independent $I_{tx,M}$ is calculated by simultaneously solving Eqns (18), (19), and (20). Therefore, when $I_{tx,M}$ and $I_{tx,opt}$ are used, the efficiency difference can explain the high-efficiency operation.

The coupling range denoted by region C of Fig. 7 means $k_1 \in [0.2, 0.34]$ and $k_2 \in [0.25, 0.45]$. It is defined as Case C, and the corresponding simulation results are shown in Fig. 8a. The left graph illustrates the coupler efficiency $\eta_{c,M}$ under excitation $I_{tx,M}$, while the right graph displays the efficiency difference $\Delta\eta_c$ between the maximum coil efficiency $\eta_{c,iopt}$ (using $I_{tx,opt}$) and $\eta_{c,M}$ (using $I_{tx,M}$). Within the coupling range, the efficiency difference is less than 0.2%. As shown in Fig. 8b, with a further expansion of the coupling range in Case D ($k_1 \in [0.1, 0.34]$, $k_2 \in [0.15, 0.45]$), the maximum efficiency drop is 0.8%. From these examples, it is evident that adopting the proposed current would maintain relatively high coupler efficiency without dramatically increasing the requirement of real-time coupling information.

Experimental verification

An experimental platform was implemented using a single-TX dual-RX system to validate the theoretical conclusion. As illustrated in Fig. 9 the setup includes a DC source, a full-bridge inverter, a large square TX coil, two small RX coils (rectangular RX1 and square RX2), rectifiers, and loads. The TX side employs an LCC compensation structure, while the RX sides utilize series compensation. This compensation is convenient to use the DC input voltage for the TX coil current control due to the clamping effect. The coil

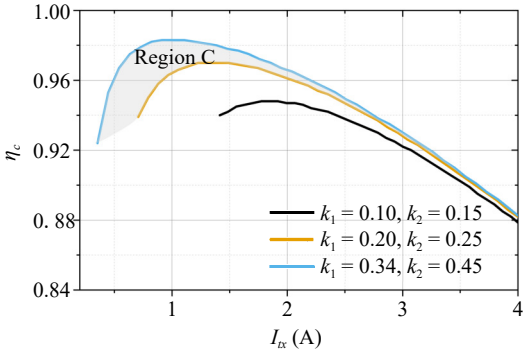

Fig. 7 Coupler efficiency of a 2-RX system under different coupling conditions.

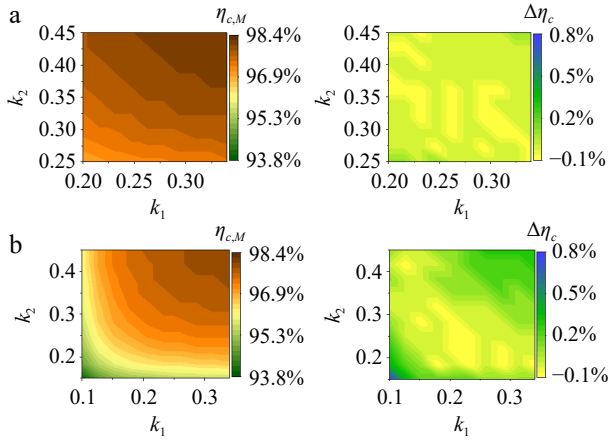

Fig. 8 Efficiency comparison. (a) Case C: $\eta_{s,M}$ (left), $\Delta\eta_c$ (right); (b) $\Delta\eta_c$ (left), $\Delta\eta_c$ (right).

parameters are provided in Table 1, and the compensation parameters are as follows: L_t = 32 μH, C_t = 110 nF, C_{tx} = 57 nF, C_{rx1} = 227 nF, C_{rx2} = 132.8 nF. The charging powers for the two loads are P_1 = 10 W and P_2 = 15 W.

When two RXs are placed within a specific charging area in Fig. 9 (i.e., not moving outside the TX), the coupling variation ranges are measured as $k_1 \in [0.26, 0.34]$ and $k_2 \in [0.31, 0.45]$. Using the driving current Eqn (20), with an effective value of $I_{tx,M}$ = 1.151 A, a corresponding DC voltage of V_{dc} = 23 V is provided. Note that the coil current is clamped by the input DC voltage in LCC compensation. Within the mentioned coupling variation range and power demands, the experimental waveforms of inverter output voltage v_{in}, input current i_{in}, and TX coil input current i_{tx} are depicted in Fig. 10. When employing $I_{tx,M}$, v_{in}, and i_{tx} remain constant, while i_{in} exhibits slight fluctuations under coupling variation.

The efficiency analysis in the preceding section exclusively concentrates on the coupler itself, but the efficiency is also influenced by compensations, inverters, and rectifiers. And the characteristic traits of the efficiency curve primarily stem from the attributes of the coupler. Past studies have emphasized that a precise analysis of system efficiency necessitates the consideration of all loss models. However, when optimizing efficiency, the control mechanisms often resort to simplified analyses to deduce the terminal requisites for the resonant tank. Hence, in the ensuing analysis, a comprehensive system-level evaluation could be undertaken to yield results akin to those illustrated in Figs 7 and 8.

Similar to the AC simulation in Fig. 7, the influence of the coupling could be studied in a complete DC to DC system. The overall efficiency η_s is measured by sweeping the input current as shown in Fig. 11. An optimal current exists, and it is still valid to have a conclusion that a stronger coupling leads to a lower optimal current.

When employing $I_{tx,M}$, as illustrated in Fig. 10, and moving two RX coils to change their coupling, the input and output power were measured using a power analyzer. The system efficiency $\eta_{s,M}$ is then obtained in Fig. 12a, which changes from 89.5% to 92.6%. Simultaneously, the optimal efficiency values $\eta_{c,sopt}$ (obtained by sweeping the input current) under different couplings are measured and compared with $\eta_{s,M}$. The difference is illustrated in Fig. 12b. At higher coupling, $\eta_{s,M}$ is closer to $\eta_{s,opt}$, differing by only 0.4%. As the coupling weakens, the efficiency difference gradually increases, reaching a maximum of 1.7%. The proposed control can maintain high-efficiency operations without the need for coupling estimation.

The similar trends in simulation and experiment indicate that the differences in efficiency are mainly attributed to the losses in the active circuits (inverter and rectifier) and conductor losses. The AC analysis in the previous sections would be used to guide the current control in a complete DC-to-DC system. The experimental results demonstrate that the proposed excitation based on the coupling range maintains a certain level of high efficiency, with stable input and simple control strategies.

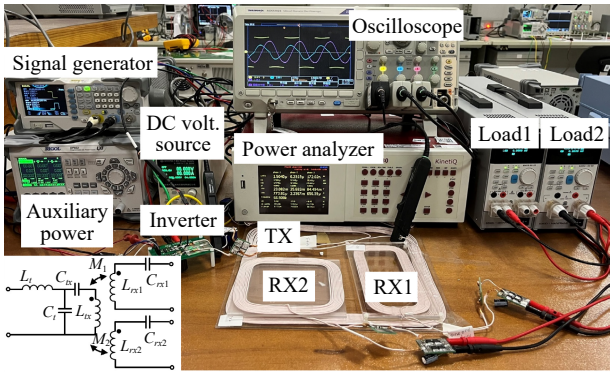

Fig. 9 Experimental setup.

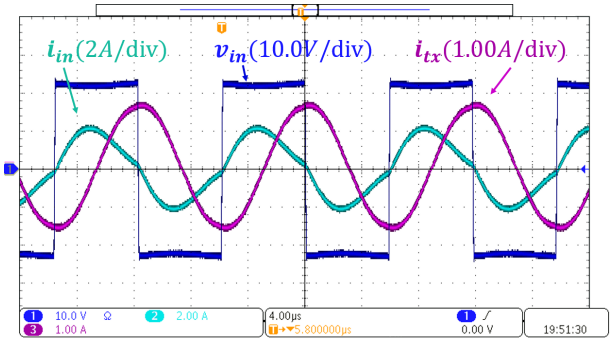

Fig. 10 Experimental waveform.

Conclusions

This paper proposes a simple driving logic to dramatically improve the scalability of a general single-TX multi-RX IPT system. The high-efficiency operation is achieved without knowing the real coupling and does not suffer from the coupling variation issue. Using the one-RX example, the coupler analysis unified the understanding of optimal conditions, which serves as the reference to justify the benefit of the proposed excitation. The same control logic is then extended to a general multi-RX case based on the derivation of optimal conditions. The claimed benefit is finally verified in a complete two-RX system.

Author contributions

The authors confirm contribution to the paper as follows: theoretical derivation, experimental validation, and manuscript writing: Wang X, He R; manuscript writing: Lin Z; conceptualization, funding acquisition, and supervision: Fu M. All authors reviewed the results and approved the final version of the manuscript.

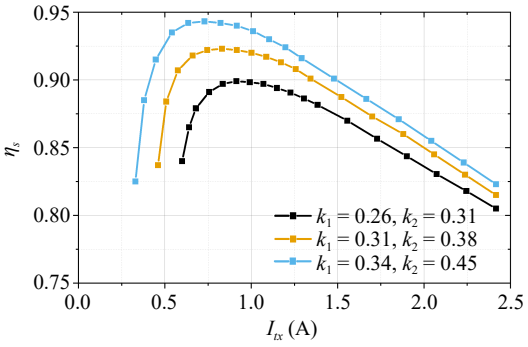

Fig. 11 Efficiency under different coupling conditions.

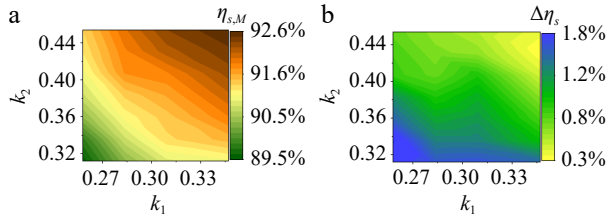

Fig. 12 (a) System efficiency $\eta_{s,M}$. (b) Efficiency drop: $\Delta\eta_s = \eta_{s,opt} - \eta_{s,M}$.

Data availability

The datasets generated during and/or analyzed during the current study are available from the corresponding author on reasonable request.

Acknowledgments

This work was supported by National Natural Science Foundation of China (Grant No. 52477013).

Conflict of interest

The authors declare that they have no conflict of interest.

Dates

Received 11 September 2024; Revised 4 December 2024; Accepted 9 December 2024; Published online 26 March 2025

References

1. Zhang Y, Chen S, Li X, Tang Y. 2022. Design methodology of free-positioning nonoverlapping wireless charging for consumer electronics based on antiparallel windings. *IEEE Transactions on Industrial Electronics* 69:825–34
2. Chen W, Lu W, lu HH-C, Fernando T. 2020. Compensation network optimal design based on evolutionary algorithm for inductive power transfer system. *IEEE Transactions on Circuits and Systems I: Regular Papers* 67:5664–74
3. Tan T, Chen K, Lin Q, Jiang Y, Yuan L, et al. 2021. Impedance shaping control strategy for wireless power transfer system based on dynamic small-signal analysis. *IEEE Transactions on Circuits and Systems I: Regular Papers* 68:1354–65
4. Lu J, Zhu G, Mi CC. 2022. Foreign object detection in wireless power transfer systems. *IEEE Transactions on Industry Applications* 58:1340–54
5. Ahn D, Kim SM, Kim SW, Moon JI, Cho IK. 2019. Wireless power transfer receiver with adjustable coil output voltage for multiple receivers application. *IEEE Transactions on Industrial Electronics* 66:4003–12
6. Cheng C, Li W, Zhou Z, Deng Z, Mi C. 2020. A load-independent wireless power transfer system with multiple constant voltage outputs. *IEEE Transactions on Power Electronics* 35:3328–31
7. Cheng C, Lu F, Zhou Z, Li W, Deng Z, et al. 2020. A load-independent lcc-compensated wireless power transfer system for multiple loads with a compact coupler design. *IEEE Transactions on Industrial Electronics* 67:4507–15
8. Song J, Liu M, Ma C. 2020. Analysis and design of a high-efficiency 6.78-MHz wireless power transfer system with scalable number of receivers. *IEEE Transactions on Industrial Electronics* 67:8281–91
9. Lee SB, Kim M, Jang IG. 2021. Determination of the optimal resonant condition for multireceiver wireless power transfer systems considering the transfer efficiency and different rated powers with altered coupling effects. *IEEE Journal of Emerging and Selected Topics in Power Electronics* 9:2384–93
10. Liu F, Yang Y, Ding Z, Chen X, Kennel RM. 2018. A multifrequency superposition methodology to achieve high efficiency and targeted power distribution for a multiload MCR WPT system. *IEEE Transactions on Power Electronics* 33:9005–16
11. Huang Y, Liu C, Xiao Y, Liu S. 2020. Separate power allocation and control method based on multiple power channels for wireless power transfer. *IEEE Transactions on Power Electronics* 35:9046–56
12. Luo C, Qiu D, Gu W, Zhang B, Chen Y, et al. 2022. Multiload wireless power transfer system with constant output power and efficiency. *IEEE Transactions on Industry Applications* 58:1101–14
13. Kim JW, Hwang IJ, Yu JW, Yeo TD. 2021. Maximum efficiency point tracking scheme for loosely coupled multiple-receiver wireless power charging system with mutual inductance tracking. *IEEE Transactions on Microwave Theory and Techniques* 69:378–86
14. Fu M, Yin H, Liu M, Wang Y, Ma C. 2018. A 6.78 MHz multiple-receiver wireless power transfer system with constant output voltage and optimum efficiency. *IEEE Transactions on Power Electronics* 33:5330–40
15. Zhao P, Ji X, Wang H, Fu M. 2023. H5-bridge-based bowl-shape wireless charger for multiple loads. *IEEE Transactions on Industrial Electronics* 70:8853–61
16. Fu M, Yin H, Zhu X, Ma C. 2015. Analysis and tracking of optimal load in wireless power transfer systems. *IEEE Transactions on Power Electronics* 30:3952–63
17. Zhong WX, Hui SYR. 2015. Maximum energy efficiency tracking for wireless power transfer systems. *IEEE Transactions on Power Electronics* 30:4025–34
18. Diekhans T, De Doncker RW. 2015. A dual-side controlled inductive power transfer system optimized for large coupling factor variations and partial load. *IEEE Transactions on Power Electronics* 30:6320–28
19. Berger A, Agostinelli M, Vesti S, Oliver JA, Cobos JA, et al. 2015. A wireless charging system applying phase-shift and amplitude control to maximize efficiency and extractable power. *IEEE Transactions on Power Electronics* 30:6338–48
20. Dai X, Li X, Li Y, Hu AP. 2018. Maximum efficiency tracking for wireless power transfer systems with dynamic coupling coefficient estimation. *IEEE Transactions on Power Electronics* 33:5005–15
21. Li H, Li J, Wang K, Chen W, Yang X. 2015. A maximum efficiency point tracking control scheme for wireless power transfer systems using magnetic resonant coupling. *IEEE Transactions on Power Electronics* 30:3998–4008
22. Fu M, Zhang T, Ma C, Zhu X. 2015. Efficiency and optimal loads analysis for multiple-receiver wireless power transfer systems. *IEEE Transactions on Microwave Theory and Techniques* 63:801–12